New Phytologist

Research

Ocean acidification alters the nutritional value of Antarctic diatoms

Rebecca J. Duncan[1,2], Daniel A. Nielsen[1], Cristin E. Sheehan[1,3], Stacy Deppeler[4,5], Alyce M. Hancock[4,6,7], Kai G. Schulz[8], Andrew T. Davidson[7,9] and Katherina Petrou[1]

[1]School of Life Sciences, University of Technology Sydney, Sydney, NSW 2007, Australia; [2]Department of Arctic Biology, The University Centre in Svalbard, Longyearbyen 9171, Norway; [3]Climate Change Cluster, University of Technology Sydney, Sydney, NSW 2007, Australia; [4]Institute for Marine and Antarctic Studies, University of Tasmania, Hobart, Tas. 7001, Australia; [5]National Institute of Water and Atmospheric Research, Wellington 6021, New Zealand; [6]Antarctic Gateway Partnership, Battery Point, Tas. 7004, Australia; [7]Antarctic Climate and Ecosystems Cooperative Research Centre, Hobart, Tas. 7001, Australia; [8]Centre for Coastal Biogeochemistry, Southern Cross University, East Lismore, NSW 2480, Australia; [9]Australian Antarctic Division, Department of the Environment and Energy, Hobart, Tas. 7050, Australia

Author for correspondence:
Katherina Petrou
Email: katherina.petrou@uts.edu.au

Received: *7 July 2021*
Accepted: *7 November 2021*

New Phytologist (2022) **233:** 1813–1827
doi: 10.1111/nph.17868

Key words: climate change, diatoms, FTIR microspectroscopy, macromolecules, microalgae, phytoplankton, Southern Ocean.

Summary

- Primary production in the Southern Ocean is dominated by diatom-rich phytoplankton assemblages, whose individual physiological characteristics and community composition are strongly shaped by the environment, yet knowledge on how diatoms allocate cellular energy in response to ocean acidification (OA) is limited. Understanding such changes in allocation is integral to determining the nutritional quality of diatoms and the subsequent impacts on the trophic transfer of energy and nutrients.
- Using synchrotron-based Fourier transform infrared microspectroscopy, we analysed the macromolecular content of selected individual diatom taxa from a natural Antarctic phytoplankton community exposed to a gradient of fCO_2 levels (288–1263 µatm).
- Strong species-specific differences in macromolecular partitioning were observed under OA. Large taxa showed preferential energy allocation towards proteins, while smaller taxa increased both lipid and protein stores at high fCO_2.
- If these changes are representative of future Antarctic diatom physiology, we may expect a shift away from lipid-rich large diatoms towards a community dominated by smaller taxa, but with higher lipid and protein stores than their present-day contemporaries, a response that could have cascading effects on food web dynamics in the Antarctic marine ecosystem.

Introduction

Ocean acidification (OA) is one of the most prodigious and ubiquitous threats to the structure and function of marine life (Ross *et al.*, 2011; Kroeker *et al.*, 2013; Hancock *et al.*, 2020). Since the beginning of the industrial era, the world's oceans have sequestered *c.* 30% of anthropogenic CO_2 emissions (Sabine *et al.*, 2004; Denman *et al.*, 2007; Le Quéré *et al.*, 2018). As a result, the average ocean surface water pH has fallen from *c.* 8.21 to 8.10 (IPCC, 2014), equivalent to a 29% increase in hydrogen ion (H^+) concentrations. If CO_2 emissions continue unabated (RCP8.5), atmospheric CO_2 concentrations are estimated to rise from the current *c.* 410 ppmv to > 1000 ppmv by 2100 (IPCC, 2014), with the average ocean pH expected to further decline by up to 0.4 pH units (IPCC, 2014). The cold waters of the Southern Ocean (SO) result in higher than average CO_2 uptake in this region (Khatiwala *et al.*, 2009; Frölicher *et al.*, 2015) and the naturally low saturation state (McNeil & Matear, 2008) renders the Antarctic marine ecosystem and its biota immediately vulnerable to the effects of OA.

Phytoplankton provide the nutritional base that underpins the wealth of life in the oceans. Their growth and productivity have been shown to be positively (Wu *et al.*, 2010; Tew *et al.*, 2014; Baragi *et al.*, 2015; Chen *et al.*, 2015), negatively (Chen & Durbin, 1994; Hoppe *et al.*, 2015; Shi *et al.*, 2017) and neutrally (Beardall & Raven, 2004; Berge *et al.*, 2010) affected by increased CO_2 concentrations. Similarly, no definitive taxonomic or size-related shifts in phytoplankton community composition in response to OA have been determined (Feng *et al.*, 2009, 2010; Nielsen *et al.*, 2010; Eggers *et al.*, 2014; Bach & Taucher, 2019). This variability in phytoplankton community response to CO_2 has been suggested to result from differences in the concentrations tested, for which low CO_2 enhancement promotes growth with increased passive transfer of CO_2 for photosynthesis, while higher CO_2 inhibits growth in some taxa, possibly due to high energy costs associated with greater dependence on H^+ pumps (Deppeler *et al.*, 2018; Paul & Bach, 2020). Nevertheless, the range in CO_2-driven responses to productivity and community composition, highlights the presence of interspecific differences in tolerance. Therefore, uncovering the tolerance and

thresholds of individual species is essential for understanding species and community responses to the projected OA.

In pelagic food webs, the effects of small changes in nutrient availability at the primary production level can have broad, cascading effects on higher trophic organisms (Moline *et al.*, 2001). Lipids, which are the most energy-rich macromolecules, contain much of the energy that is transferred among trophic levels (Hagen & Auel, 2001). Adequate lipid supply has been shown to be critical to the survival and reproduction of zooplankton (Graeve *et al.*, 1994; Lee *et al.*, 2006), particularly for Antarctic krill (Hagen & Auel, 2001) that require large lipid reserves over winter when primary production is scarce. Proteins are also a key source of energy (Hagen & Auel, 2001), the predominant source of amino acids (Ruess & Müller-Navarra, 2019), and a cellular nitrogen reservoir (Finkel *et al.*, 2016) for higher trophic levels. Macromolecular stores of primary producers are the cornerstone of productive marine ecosystems and changes in the partitioning of critical macromolecules contained in phytoplankton, such as proteins and lipids, inevitably alters the supply of energy and essential compounds to higher trophic levels.

Diatoms dominate much of the primary production in the SO (Wright *et al.*, 2010; Wolf *et al.*, 2013; Eggers *et al.*, 2014), particularly in coastal areas and along sea ice margins (Kang & Fryxell, 1993; Wright *et al.*, 2010). Diatoms form dense, siliceous cell walls known as frustules by converting soluble silicic acid into biogenic silica (Martin-Jézéquel *et al.*, 2000). These frustules provide the cell with ballast (Tréguer *et al.*, 2018), and afford the cell some defence against grazers (Hamm *et al.*, 2003). Despite this protective armour, the relatively high growth rates and generally larger cell sizes make diatoms a favourite food source for krill and other large zooplankton, delivering both quality and quantity of proteins and lipids necessary for growth and reproduction (Cowles *et al.*, 1988; Litchman *et al.*, 2007; Bhavya *et al.*, 2018). Indeed, Antarctic krill and copepods have been shown to selectively feed on diatoms (Cowles *et al.*, 1988; Head & Harris, 1994; Turner *et al.*, 2001; Haberman *et al.*, 2003) with a strong preference for less silicified diatoms, which has been shown to benefit copepod growth rate, egg production and hatching (Liu *et al.*, 2016). Enrichment of seawater with CO_2 has been shown to stimulate carbon fixation in diatoms, thereby reducing the nutrient content relative to carbon (Urabe *et al.*, 2003; Bellerby *et al.*, 2008; Engel *et al.*, 2008) and therefore food quality for zooplankton, yet little information is known about the effects of OA on diatom macromolecular composition. In one study, acidification (750 μatm) resulted in a decline in total fatty acids (FAs) in the discoid centric diatom *Thalassiosira weissflogii* that translated to a 10-fold decline in FAs in the fed copepods, causing significant declines in copepod somatic growth and egg production (Rossoll *et al.*, 2012). Given the importance of the diatom–zooplankton link in the Antarctic pelagic food web, these results emphasise the importance for understanding how OA may influence the nutritional quality of key primary producers.

Understanding which species within the phytoplankton community are affected by environmental change requires a depth of study that broader community analyses do not provide. Single-cell analyses on natural mixed communities provides a unique insight into the extent to which a member of the community is affected, delivering unprecedented detail on potential physiological and ecological implications. In a parallel study on the same phytoplankton community, we used single-cell analyses to investigate the effects of OA on the silicification rates of several Antarctic marine diatoms from within a natural mixed community (Petrou *et al.*, 2019). This study uncovered species-specific sensitivities to acidification and revealed a potential threat of OA to diatoms. In another study, single-cell analyses were used to differentiate diatoms from contrasting Antarctic marine habitats based on the taxonomic-specific macromolecular fingerprint (Sheehan *et al.*, 2020). However, to date, no study has looked at the macromolecular profiles of individual diatoms from a natural, phytoplankton assemblage in response to increasing CO_2 concentration. Knowledge of species-specific macromolecular partitioning under high CO_2 may help to elucidate potential changes to the nutritional quality of primary producers and in combination with information on lower trophic feeding links, may refine our understanding of the role of diatoms in secondary production.

Using synchrotron-based Fourier transform infrared (FTIR) microspectroscopy, we determined the macromolecular composition of selected Antarctic marine diatoms from amongst a natural community following a 18-d exposure to different fCO_2 levels, delivering a snapshot of carbon partitioning as a response to OA. In our experiment, large volume mesocosms were used, ensuring the inclusion of the entire microbial community – phytoplankton, bacteria, viruses – and the influence of these interactions (predation, competition) among and between these trophic levels, improving our ability to extrapolate to natural systems (Cottingham *et al.*, 2005; Kreyling *et al.*, 2018). Furthermore, by exposing the communities to a gradient of increasing fCO_2, we enhanced the predictive strength of our data (Havenhand *et al.*, 2010). Through single-cell analyses, we showed differential effects of OA on the partitioning of macromolecules by individual diatom taxa, offering insight into potential implications of fCO_2-induced changes to energy availability and transfer through the Antarctic marine food web.

Materials and Methods

Experimental design and mesocosm set-up

Mesocosm set-up and conditions were as described previously (Deppeler *et al.*, 2018; Hancock *et al.*, 2018; Petrou *et al.*, 2019; Supporting Information Table S1). Briefly, a near-shore, natural Antarctic microbial community was collected from an ice-free area among broken fast ice *c.* 1 km offshore from Davis Station, Antarctica (68°35′S, 77°58′E) on 19 November 2014. This community was incubated in 6 × 650 l polyurethane tanks (mesocosms) across a gradient of fCO_2 levels (343, 506, 634, 953, 1140 and 1641 μatm; denoted M1–M6). These fCO_2 levels corresponded to pH values ranging from 8.17 to 7.57 (Table S1). The seawater was initially gravity fed through a 200 μm Arkal filter to exclude metazooplankton. Unavoidably, this filtration may also have removed some of the larger chain-forming diatom taxa as well. Temperature was maintained at 0.0 ± 0.5°C and the mesocosms were stirred continuously by a central auger (15 rpm)

for gentle mixing and covered with an air-tight lid. Irradiance was initially kept low (0.8 ± 0.2 µmol photons m^{-2} s^{-1}), while cell physiology was left to acclimate to increasing fCO_2 levels (over 5 d). When target fCO_2 levels were reached in all six mesocosms, light was gradually increased (days 5–8) to 89 ± 16 µmol photons m^{-2} s^{-1} on a 19 h : 5 h, light : dark cycle, to mimic current natural conditions. To generate the gradient in carbonate chemistry, filtered seawater saturated with CO_2 was added to five of the mesocosms. One mesocosm remained at ambient levels, with regular filtered seawater (unenriched with CO_2), to control for the physical disturbance and dilution from the CO_2-enriched seawater additions to the other mesocosms. Daily measurements were taken to monitor pH and dissolved inorganic carbon (DIC). The former was measured using the indicator dye *m*-cresol purple on a GBC UV-vis 916 spectrophotometer in a 10 cm temperature-controlled (25°C) cuvette (Dickson *et al.*, 2007). DIC was measured on an Apollo SciTech AS-C3 by infrared absorption and calibrated against certified reference material batch CRM127 (Dickson, 2010). Practical alkalinity (PA) was calculated at 25°C, as per Deppeler *et al.* (2018). For details of fCO_2 manipulations, analytical procedures and calculations see Deppeler *et al.* (2018). Samples for physiological and macromolecular measurements in this study were taken on day 18, at the end of the incubation period (Deppeler *et al.*, 2018).

Macronutrient analyses

Samples for macronutrient concentration for this study were obtained from each mesocosm on day 18, filtered through 0.45-µm cellulose ester filters (Millipore) and frozen at −20°C. Concentrations of nitrate/nitrite (NO_x), soluble reactive phosphorus (SRP) and molybdate reactive silica (Silica) were determined following analysis described previously (Davidson *et al.*, 2016). Operational detection limits for NO_x, SRP and Silica were 0.14, 0.10 and 1.66 µM, respectively.

Diatom community structure

Samples for community structure and abundance were collected from each mesocosm on days 1, 3, 5, 8, 10, 12, 14, 16 and 18. These were microscopically analysed within 2 yr of collection as described in Hancock *et al.* (2018). Briefly, between 2 and 10 ml of refrigerated Lugol's concentrated fixed samples were placed in an Utermöhl cylinder (Hydro-Bios, Altenholz, Germany) and cells allowed to settle overnight. A stratified counting procedure was used to capture both small and large cells, with all cells > 20 µm identified and quantified at ×200 magnification, while those < 20 µm were assessed at ×400 magnification. Size categories were established via visual inspection with assistance of a graticule in the ocular or the light microscope. To determine growth condition (active or stationary) closest to time of macromolecular profiling (day 18), cell counts from days 14 to 18 for each taxon from each mesocosm (Hancock *et al.*, 2018) were used to estimate specific growth rates on day 18 (for complete growth curves, see Hancock *et al.*, 2018). Due to limitations in species identification for some taxa during FTIR microspectroscopy measurements, some species were grouped. Selected taxa for determination of macromolecular composition in this study included *Chaetoceros* spp. (predominantly comprised of chains of *C. castracanei*, but also *C. tortissimus* and *C. bulbosus*), *Fragilariopsis cylindrus*, *Proboscia truncata*, *Stellarima microtrias* and large discoid centric (> 20 µm) diatoms (including *Thalassiosira ritscheri* and unidentified large discoid centric diatoms (> 20 µm), predominantly from the genus *Thalassiosira*). These taxa were selected for analyses, as they were the most prevalent large (> 10–15 µm) diatoms to be found in all six tanks (Hancock *et al.*, 2018; Table S3) and together, they represent up to 11% of the diatom dominated community (Table S3; Hancock *et al.*, 2018). While their numerical contribution may be relatively minor, being the largest cells within the community, their contribution to the community macromolecular pool is significant. Furthermore, in analysing multiple taxa, we can uncover potential response diversity of macromolecular partitioning in diatoms to OA.

Cell volume and photophysiological status

Cell volume was determined for selected taxa from M1 and M6 via light microscopy. Cells were imaged on a calibrated microscope (Nikon Eclipse Ci-L, Tokyo, Japan) and length, width and height (24–77 cells per taxa) determined using ImageJ software (Schneider *et al.*, 2012). Biovolume was then calculated according to the cell morphology and corresponding equations described by Hillebrand *et al.* (1999). To establish photophysiological status of individual taxa, maximum quantum yield of Photosystem II (F_V/F_M) was measured on individual cells as described in Petrou *et al.* (2019). Briefly, mesocosm samples were loaded into a flow cell (Bioptech, Butler, PA, USA) and chlorophyll *a* fluorescence measurements made on randomly selected diatom cells using a pulse amplitude modulated fluorometer (Imaging PAM IMAG-K4; Walz GmbH, Effeltrich, Germany) mounted on a compound microscope (Axiostar plus, Zeiss, Germany). Following 10 min dark-adaptation, minimum fluorescence was recorded and then a saturating pulse of light was applied (SP width = 0.8 s; SP intensity = 10; using the special SP-routine) to obtain maximum fluorescence. From these two parameters F_V/F_M was calculated. All measurements were taken at ×200 magnification, with blue excitation light (440 nm) and at 0°C.

Species-specific macromolecular content by FTIR

The macromolecular composition of the selected diatom taxa sampled from all six mesocosms on day 18 was determined using synchrotron-based FTIR microspectroscopy on formalin-fixed (2% v/v final concentration) cells. Samples were fixed directly after being taken from the mesocosm, kept refrigerated and analysed within 9 months. Measurements were made on hydrated cells, a method shown to limit light-scattering effects (Bambery *et al.*, 2012) and processed according to previous studies (Sackett *et al.*, 2013, 2014; Sheehan *et al.*, 2020). Briefly, fixed cells were loaded directly onto a microcompression cell with a 0.3 mm thick CaF_2 window (Tobin *et al.*, 2010). Spectral data of individual cells (between 15 and 49 cells per taxon per mesocosm; Table S2) were collected in transmission mode, using the Infrared

Microspectroscopy Beamline at the Australian Synchrotron, Melbourne, in November 2015. Spectra (one per cell) were acquired over the measurement range 4000–800 cm^{-1} with a Vertex 80v FTIR spectrometer (Bruker Optics, Ettlingen, Germany) in conjunction with an FT-IR microscope (Hyperion 2000; Bruker) fitted with a mercury cadmium telluride detector cooled with liquid nitrogen. To reduce water vapour interference, the microscope stage was contained within a box flushed with dehumidified air. Co-added interferograms ($n = 64$) were collected at a wavenumber resolution of 6 cm^{-1} s. To allow for measurements of individual cells, all measurements were made in transmission mode, using a measuring area aperture size of 5 × 5 µm. Spectral acquisition and instrument control were achieved using OPUS 6.5 software (Bruker). All cells were identified and inspected visually to ensure consistency across spectral measurements. In cases in which the taxon was much larger than the aperture, three scans from different areas of the cell were taken and averaged, ensuring full coverage of cellular components.

Normalised spectra of biologically relevant regions revealed absorbance bands representative of key macromolecules, from which five previously verified band assignments were selected for comparison within taxon and treatment (Table 1). In this study, the amide II band (*c.* 1540 cm^{-1}) was used as an indicator of cellular protein content, as the other major protein band, amide I was masked by water absorption. Lipids were primarily determined using the integrated peak of the ester carbonyl from lipids (*c.* 1745 cm^{-1}) as described previously (Heraud *et al.*, 2005), but with associated changes to saturated FAs. Carbohydrates were not measured, as the silica from diatoms overlaps with these bands.

Data analyses

Infrared spectral data were analysed using custom-made scripts in R (R Core Team, 2021). The regions of 3050–2800, 1770–1100 cm^{-1}, which contain the major biological bands (Table 1), were selected for analysis. Spectral data were smoothed (4 pts either side) and second derivative (third order polynomial) transformed using the Savitzky–Golay algorithm from the PROSPECTR package in R (Stevens & Ramirez Lopez, 2013) and then normalised using the method of Single Normal Variate. Macromolecular content for individual taxon was estimated based on integrating the area under each assigned peak (Table 1), providing metabolite content according to the Beer–Lambert law, which assumes a direct relationship between absorbance and relative analyte concentration (Wagner *et al.*, 2010). Regression analyses were used to explore the functional relationships between fCO_2 and macromolecular content. Because of their superior interpolation potential, gradient designs are generally considered more useful for model parameterisation (Havenhand *et al.*, 2010). They are also deemed more effective at exposing response patterns to environmental perturbation than replicated designs (Cottingham *et al.*, 2005; Riebesell & Gattuso, 2015; Kreyling *et al.*, 2018). Integrated peak areas provide relative changes in macromolecular content between samples. Because of the differences in absorption properties of macromolecules, peak areas can only be used as relative measure within compounds. Therefore, peak areas were visualised using free axes to improve readability and discourage comparison between macromolecules. To determine significant relationships between macromolecular content and fCO_2 level, a linear regression at each fCO_2 level (±95% confidence interval) was applied to each taxon. In cases in which the data were poorly explained by a linear fit, a second order polynomial regression was applied. The Shapiro–Wilks (Shapiro & Wilk, 1965) test for normality showed that the data required log_{10} transformation before analysis. Regressions were tested for overall model significance using the, F statistic ($P < 0.05$) and strength of fit using R^2. The residuals of all regressions were verified for homoscedasticity. All analyses were performed using RSTUDIO v.1.3.959 (R Core Team, 2021) and the add-on packages GGPLOT2 v.2.2.1 (Wickham, 2009) and DPLYR v.1.0.0 (Wickham *et al.*, 2020).

Results

Chemistry, cell density and photophysiology

There was significant drawdown of macronutrients from phytoplankton growth in the mesocosms by day 18. NO_x concentration began to decline from day 10, but did not fall below the limits of detection in any tank until day 18 (Deppeler *et al.*, 2018). By day 18, SRP was lowest (0.10 µM) in M1 (control) and highest (0.19 µM) in M6 (highest fCO_2 treatment), while silica concentrations ranged from 85 µM (M3) to 99 µM (M6). DIC concentrations ranged from 2179 to 2360 µmol kg^{-1} (M1–M6, respectively), matching a gradient in total pH from 8.17 to 7.57, while PA remained relatively consistent across the pH gradient, dropping only 10 µmol kg^{-1} (Table S1). Salinity and temperature were consistent across all mesocosms (Table S1).

Table 1 Infrared band assignments for Fourier transform infrared microspectroscopy used in this study.

Wave number (cm^{-1})	Frequency range (cm^{-1})	Assignment	Compound label	Reference
c. 2920	2939–2912	ν_{as}(C–H) from methylene ($-CH_2$)	Saturated fatty acids	Vongsvivut *et al.* (2012)
c. 1745	1745–1734	ν(C=O) of ester functional groups, from membrane lipids and fatty acids	Ester carbonyl	Murdock & Wetzel (2009); Vongsvivut *et al.* (2012)
c. 1545	1556–1540	δ(N–H) of amides associated with protein	Protein (amide II)	Giordano *et al.* (2001)
c. 1452	1457–1446	$\delta_{as}(CH_3)$ and $\delta_{as}(CH_2)$ of proteins	Free amino acid	Petrou *et al.* (2018)
c. 1375	1340–1407	$\Delta_s(CH_3)$ and $\delta_s(CH_2)$ of proteins, and ν_s(C–O) of COO^- groups (carboxylic group)	Carboxylates	Giordano *et al.* (2001)

For all species except *P. truncata*, cell abundance was lowest in the highest fCO_2 treatment with a general decreasing trend with increasing fCO_2 levels following a peak density at 427 µatm (Table S3). *P. truncata* had the lowest cell abundance at 547 µatm and peak density at 957 µatm. It is important to note that the five diatom taxa selected for this study comprised < 11% of the total community in all fCO_2 treatments. Cell volume ranged from the $847 \pm 370\ \mu m^3$ for the smallest taxa, *Chaetoceros* spp., to $252\,445 \pm 180\,405\ \mu m^3$ for the largest taxa, discoid centric (> 20 µm) diatoms (Table S4). Broad indicators of the physiological state of the phytoplankton communities in the mesocosms showed that each community was photosynthetically active on day 18, where F_V/F_M values ranged between 0.61 and 0.70 (Table S3). There was however no apparent fCO_2 response.

Cell-specific macromolecular partitioning

Spectral analyses revealed taxonomic differences in macromolecular content and diverse response patterns to acidification. Between 6% and 31% of the variance in macromolecular content was found to be explained by the variation in fCO_2 (Table S5). In *Chaetoceros* spp., all investigated macromolecules showed a u-shaped response to acidification, with an initial drop in macromolecular content at moderate fCO_2 enrichment, followed by an increase towards maximum macromolecular content in cells grown at the highest fCO_2 level (Fig. 1a–e; Table S5). This u-shaped pattern, although nonsignificant, was also observed in day 18 growth rates, in which the *Chaetoceros* spp. in M3 and M4 had already entered stationary phase or were in decline (Fig. 1f). A consistent response pattern across all macromolecules was also detected for the pennate diatom *F. cylindrus*, but was the inverse of that seen for *Chaetoceros* spp., with an initial increase in macromolecular content with increased fCO_2 and generally stabilising above 700 µatm, indicating a possible threshold in fCO_2-induced synthesis of macromolecules (Fig. 2a–e; Table S5). Growth rates for *F. cylindrus* on day 18 were highest in M2–M4 and lower relative to M1 in the highest fCO_2 conditions (Fig. 2f). In *P. truncata*, a positive relationship to increasing fCO_2 was found for amide II, free amino acids and carboxylates, with minimum protein content in cells from M1 and maximum

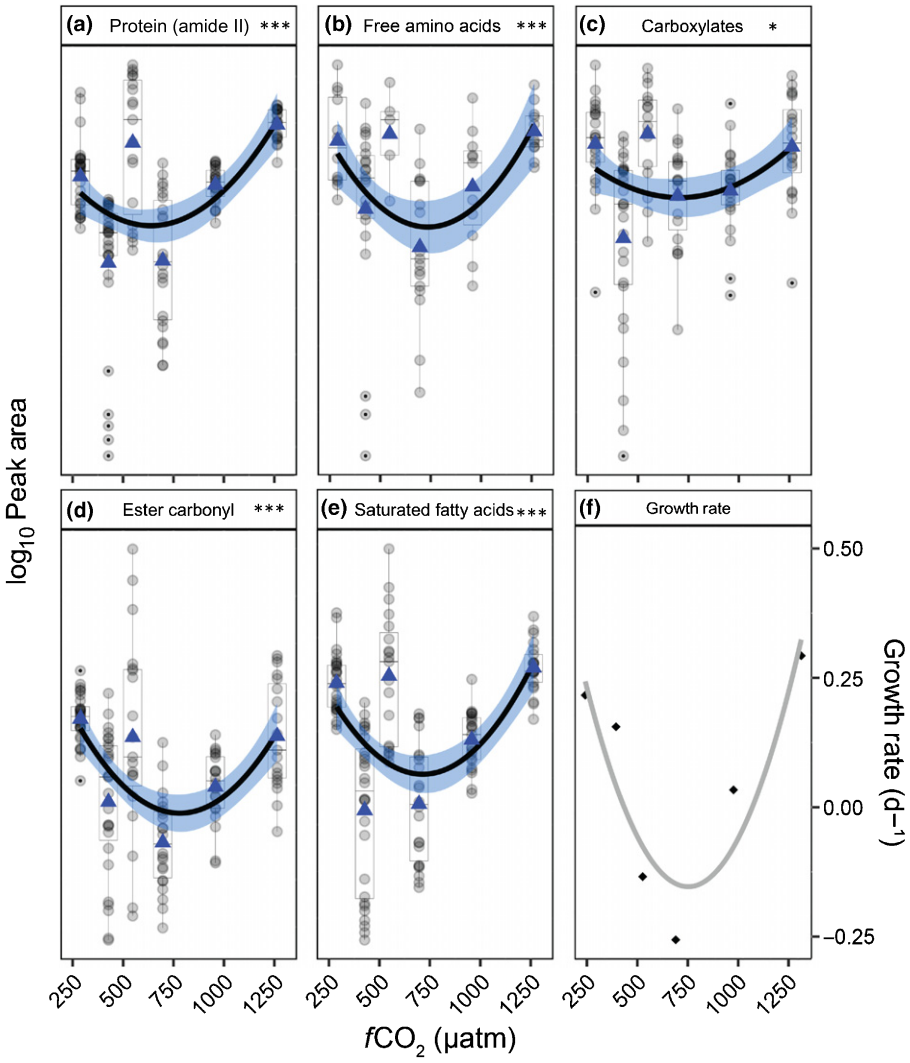

Fig. 1 Cell-specific macromolecular content (based on normalised peak areas) and growth rates for *Chaetoceros* spp. (a–f) Relative content of selected macromolecules along an fCO_2 gradient. Data are visualised using box plots with overlain grey dots showing the macromolecular content of individual cells from within fCO_2 treatment mesocosm. Data are fitted with a second order polynomial regression, with 95% confidence intervals (dark blue shading), applied to log-transformed data (*, $P < 0.05$; ***, $P < 0.0005$). The *y*-axis is free and units are arbitrary. Data means are displayed as blue triangles. (f) Growth rate (d^{-1}) is displayed as diamonds, fitted with a second order polynomial regression (grey line).

protein content in cells from M6 (Fig. 3a–c; Table S5). By contrast, ester carbonyl and saturated FAs exhibited a bell-shaped response to fCO_2, with maximal lipid content at mid-fCO_2 (Fig. 3d,e; Table S5). We observed no significant effect of fCO_2 on the growth rate of *P. truncata* (Fig. 3f).

The fCO_2-induced changes in macromolecules by the two discoid centric diatom groups, *S. microtrias* and the discoid centric group, differed greatly among compounds with strong similarities in responses of the two taxa (Figs 4, 5). For *S. microtrias*, protein from amide II exhibited a weak positive relationship ($R^2 < 0.1$), while free amino acids showed a negative relationship and carboxylates a positive relationship with increasing fCO_2 (Fig. 4a–c; Table S5). There was no response shown with saturated FAs, but a negative relationship was detected for ester carbonyl (Fig. 4d; Table S5). *S. microtrias* growth rates on day 18, showed the highest rate observed at the highest fCO_2 level (Fig. 4f). For the large discoid centric diatoms, protein showed a weak, but significant u-shaped relationship (Fig. 5a). Similar to *S. microtrias*, a negative relationship was observed in free amino acid (Fig. 5b; Table S5), while carboxylates exhibited a positive response to increasing fCO_2 (Fig. 5c; Table S5). Negative relationships were observed with both ester carbonyl and saturated FAs (Fig. 5d,e; Table S5). These changes in macromolecular content occurred despite similar growth rates at all fCO_2 concentrations (Fig. 5f).

Lipid vs protein content

To explore overall shifts in macromolecular partitioning we used the protein to lipid ratio, providing a snapshot of the principle changes to carbon allocation by the cell (Heraud *et al.*, 2005). Lipids were positively correlated with protein in *Chaetoceros* spp. (Fig. 6a; Table S6), *F. cylindrus* (Fig. 6b; Table S6) and *P. truncata* (Fig. 6c; Table S6). Despite some grouping associated with an increase in protein with the highest fCO_2 treatment, the lipid to protein ratio was largely unaffected by fCO_2 in these taxa. We found no relationship between lipid and protein content for the two large discoid centric taxa, *S. microtrias* and discoid centrics (Fig. 6d,e; Table S6).

Cell volume vs lipid and protein content

Under the lowest fCO_2 (M1), there was a positive relationship between mean taxon-specific cell volume and protein (Fig. 7a;

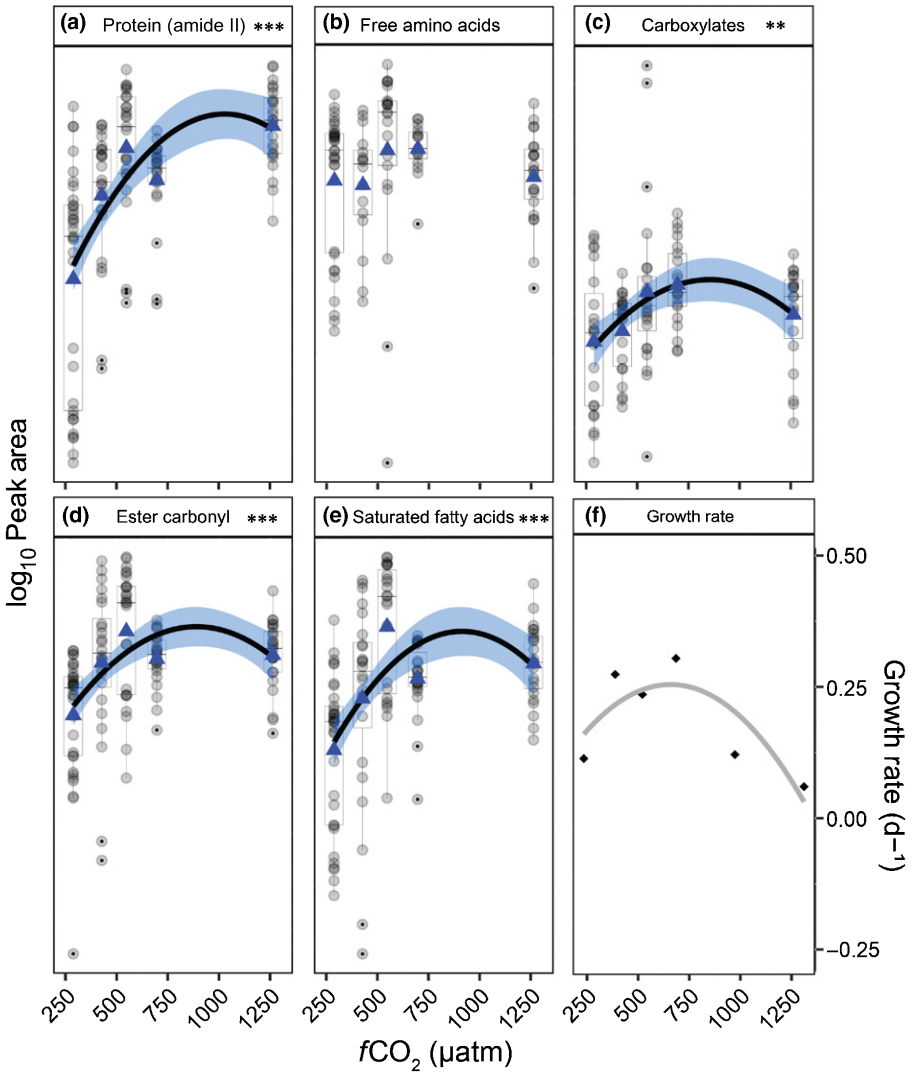

Fig. 2 Cell-specific macromolecular content (based on normalised peak areas) and growth rates for *Fragilariopsis cylindrus*. (a–f) Relative content of selected macromolecules along an fCO_2 gradient. Data are visualised using box plots with overlain grey dots showing the macromolecular content of individual cells from within fCO_2 treatment mesocosm. Data are fitted with a second order polynomial regression, with 95% confidence intervals (dark blue shading), applied to log-transformed data (**, $P < 0.005$; ***, $P < 0.0005$). The *y*-axis is free and units are arbitrary. Data means are displayed as blue triangles. (f) Growth rate (d^{-1}) is displayed as diamonds, fitted with a second order polynomial regression (grey line).

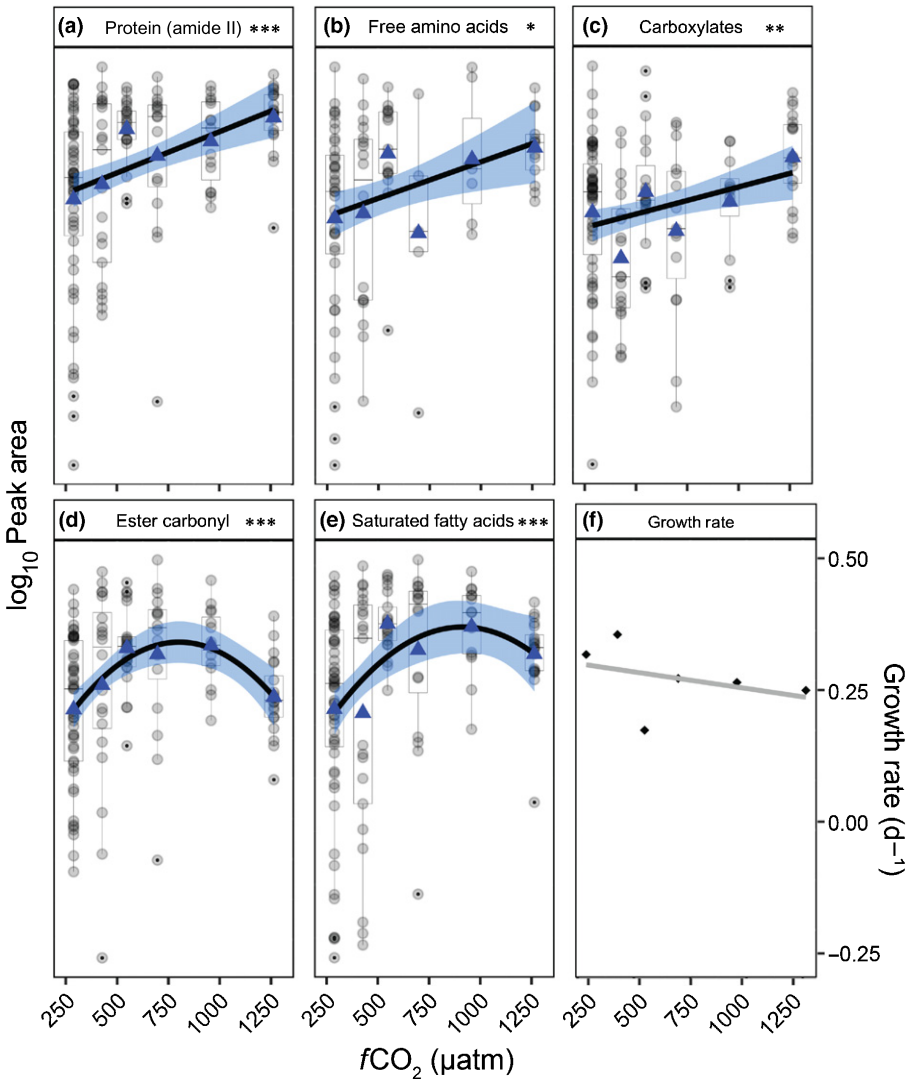

Fig. 3 Cell-specific macromolecular content (based on normalised peak areas) and growth rates for *Proboscia truncata*. (a–f) Relative content of selected macromolecules along an fCO_2 gradient. Data are visualised using box plots with overlain grey dots showing the macromolecular content of individual cells from within fCO_2 treatment mesocosm. Data are fitted with a linear or a second order polynomial regression, with 95% confidence intervals (dark blue shading), applied to log-transformed data (*, $P < 0.05$; **, $P < 0.005$; ***, $P < 0.0005$). The *y*-axis is free and units are arbitrary. Data means are displayed as blue triangles. (f) Growth rate (d^{-1}) is displayed as diamonds, fitted with linear regression (grey line).

Tables S7, S8), however no relationship was observed for lipid (ester carbonyl) content (Fig. 7b; Tables S7, S8). We did, however, find positive relationships between the mean cell volume and protein content (Fig. 7c; Tables S7, S8) and a bell-shaped relationship between mean cell volume and lipid content in the highest fCO_2 treatment (M6) (Fig. 7d; Tables S7, S8).

Discussion

The diatom–zooplankton link of the food chain is the foundation of a productive marine ecosystem, whereby changes to food quality at the primary production level can have broad consequences for energy transfer through the food web (Arrigo, 2005; Rossoll *et al.*, 2012). The effects of anthropogenic environmental change are already manifesting in some physicochemical properties of the ocean, including declining pH and increasing sea surface temperatures (Gille, 2002; IPCC, 2014). These changes are expected to be accelerated in the SO (Larsen *et al.*, 2014; Deppeler & Davidson, 2017), in which ocean pH is projected to exceed levels used in M4 before the end of the century (McNeil & Matear, 2008). OA has been shown to influence the biochemical compositions of primary producers, and their subsequent nutrient transfer to higher trophic levels, potentially disrupting marine food webs (Jin *et al.*, 2020; Nagelkerken *et al.*, 2020). This study presents a snapshot of changes to macromolecular stores in Antarctic diatoms in response to short-term exposure to increases in fCO_2. We found that elevated fCO_2 concentrations altered the way diatoms partition macromolecular content and that this partitioning differed among taxa, revealing some size-dependent relationships. Given the short duration of the study (18 d), it is unclear whether these results would be different under longer term exposure, however these data provide insight into the short-term response diversity within diatoms to acidification. Species-specific differences in resource partitioning between macromolecule storage, photosynthesis and growth, ultimately determine the quality and quantity of food available for higher trophic levels (Arrigo, 2005; Sackett *et al.*, 2016). It has been shown that acidifying ocean conditions can select for both small (< 20 μm) (Brussaard *et al.*, 2013; Hoppe *et al.*, 2013, 2017; Davidson *et al.*, 2016; Hussherr *et al.*, 2017; Sugie *et al.*, 2020)

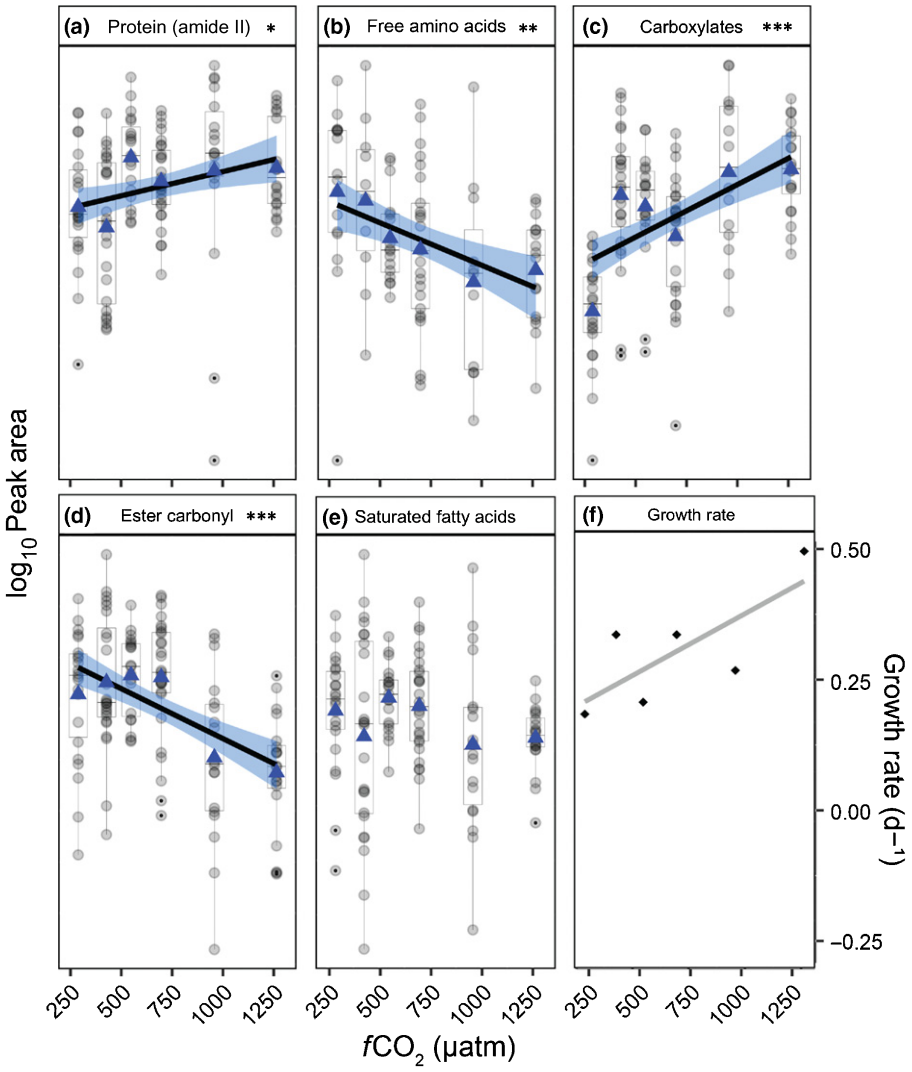

Fig. 4 Cell-specific macromolecular content (based on normalised peak areas) and growth rates for *Stellarima microtrias*. (a–f) Relative content of selected macromolecules along an fCO_2 gradient. Data are visualised using box plots with overlain grey dots showing the macromolecular content of individual cells from within fCO_2 treatment mesocosm. Data are fitted with linear regression, with 95% confidence intervals (dark blue shading), applied to log-transformed data (*, $P < 0.05$; **, $P < 0.005$; ***, $P < 0.0005$). The *y*-axis is free and units are arbitrary. Data means are displayed as blue triangles. (f) Growth rate (d^{-1}) is displayed as diamonds, fitted with linear regression (grey line).

and large (> 20 µm) diatoms (Tortell *et al.*, 2008; Feng *et al.*, 2010; Eggers *et al.*, 2014; Bach & Taucher, 2019), depending on the starting community, duration of exposure and CO_2 concentrations, and SO taxa appear to be more sensitive to these OA effects than equivalent Arctic taxa (Hoppe *et al.*, 2015). In light of the evidence that OA will select for particular phytoplankton taxa and/or size class (Hancock *et al.*, 2018; Sugie *et al.*, 2020), size-related changes to macromolecular stores could have significant implications for the trophic transfer of energy and nutrients through the marine food web.

In all five diatom groups, we saw an increase in protein content between M1 and M6. For *P. truncata* and *S. microtrias* the increase was linear, however for *F. cylindrus* the increase was linear only until M3, after which it plateaued. Both *Chaetoceros* spp. and the discoid centric group had highest protein content in M6, however they exhibited a u-shaped response to increasing fCO_2. The unexpected trend towards decline in growth rate despite increased protein content observed in *F. cylindrus*, may suggest increased energy use for protein synthesis and growth under higher fCO_2. This seems counterintuitive, as increasing CO_2 has previously been shown to reduce gross metabolism in constantly growing diatoms (Hennon *et al.*, 2015) because of the energy savings associated with downregulation of CCM activity (Hennon *et al.*, 2015, 2017), but this response may only hold true under low–moderate CO_2 enrichment (Deppeler *et al.*, 2018). Carboxylates and amino acids are the major functional groups associated with cellular protein (Bromke, 2013). We saw similar responses for carboxylate content to increasing fCO_2 in all taxa and consistent trends, within taxa, between free amino acids and proteins for *Chaetoceros* spp., and *P. truncata*, reflecting the role of amino acids in the synthesis of proteins and as precursors for metabolites with multiple functions in growth (Bromke, 2013). For the larger diatoms, *S. microtrias* and the discoid centric group, amino acids declined. Larger diatoms generally have substantial amino acid pools relative to protein content, in which amino acids can act as a nitrogen reservoir when availability is limiting (Admiraal *et al.*, 1986). Therefore, the decline of free amino acids with increasing fCO_2 in the larger diatoms could suggest use of this nitrogen reservoir for protein generation (Dortch, 1982; Marañón *et al.*, 2013). Because protein content in primary producers is an important source of energy and amino acids for higher trophic levels, ecologically, its overall increase

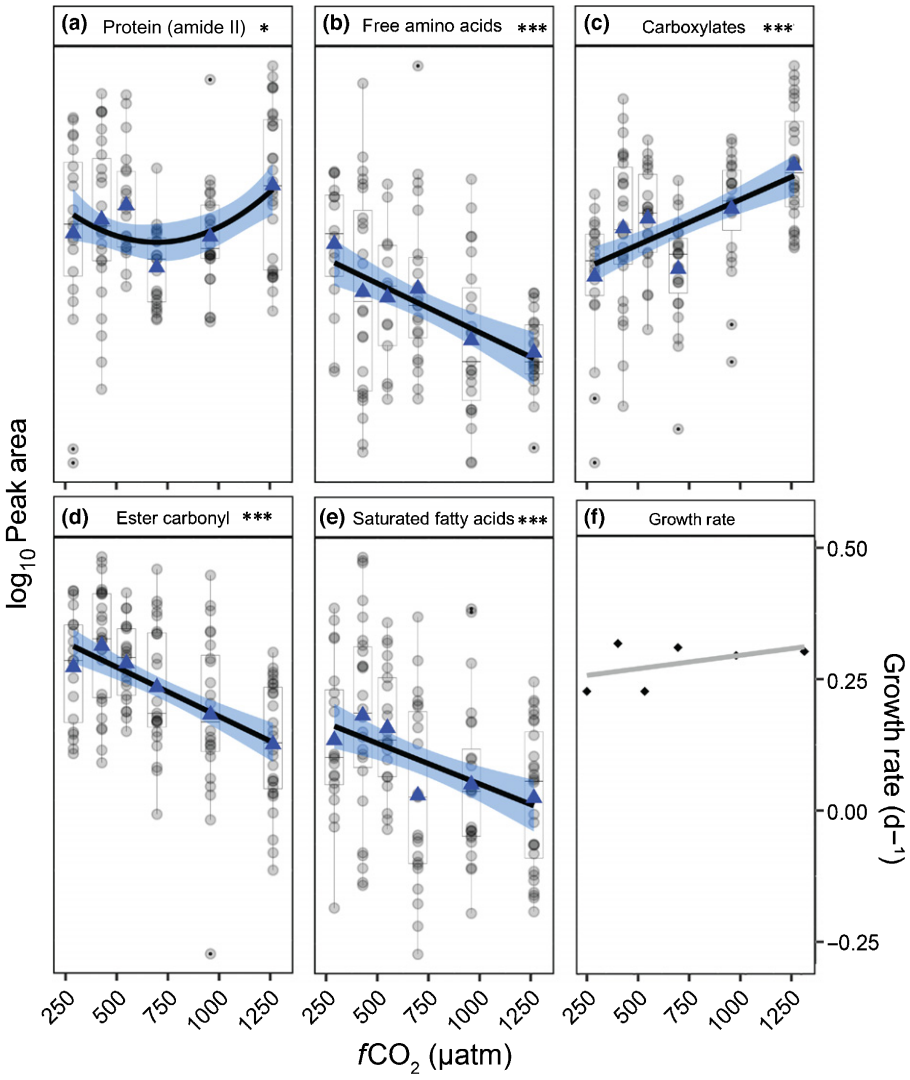

Fig. 5 Cell-specific macromolecular content (based on normalised peak areas) and growth rates for discoid centric diatoms > 20 µM. Relative content of selected macromolecules along an fCO_2 gradient. Data are visualised using box plots with overlain grey dots showing the macromolecular content of individual cells from within fCO_2 treatment mesocosm. Data are fitted with linear or second order polynomial regression, with 95% confidence intervals (dark blue shading), applied to log-transformed data (*, $P < 0.05$; ***, $P < 0.0005$). The *y*-axis is free and units are arbitrary. Data means are displayed as blue triangles. (f) Growth rate (d^{-1}) is displayed as diamonds, fitted with linear regression (grey line).

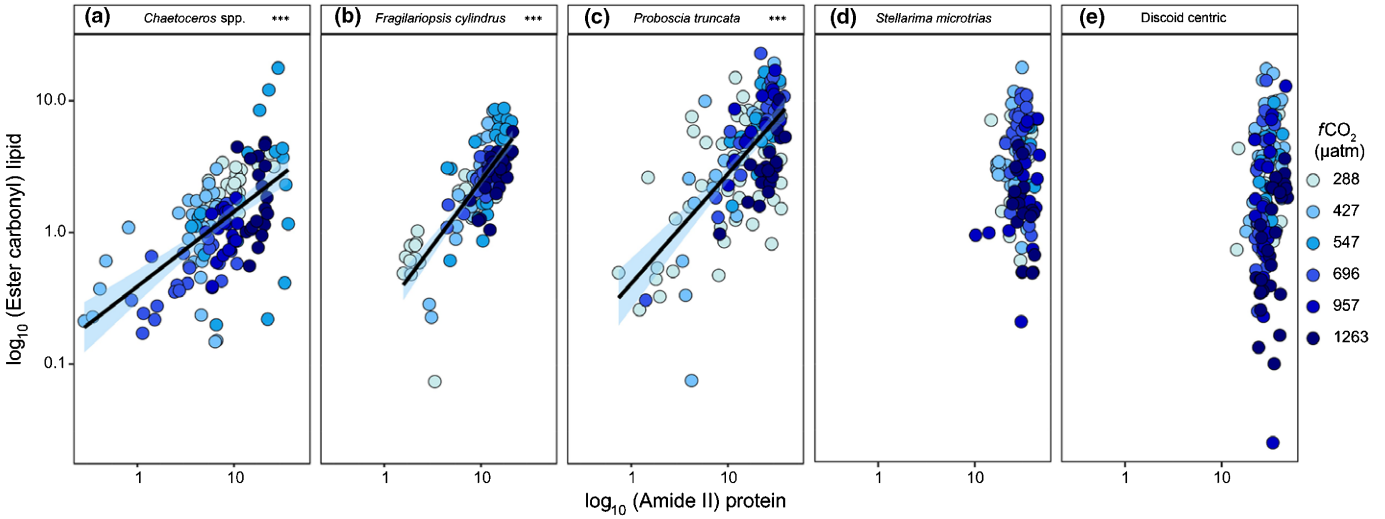

Fig. 6 Lipid (ester carbonyl) to protein (amide II) ratios for (a) *Chaetoceros* spp., (b) *Fragilariopsis cylindrus*, (c) *Proboscia truncata*, (d) *Stellarima microtrias* and (e) discoid centric diatoms > 20 µM. All data are log_{10} transformed. fCO_2 (µatm) levels are represented by colour. Data are fitted with linear regression, with 95% confidence intervals (blue shading).

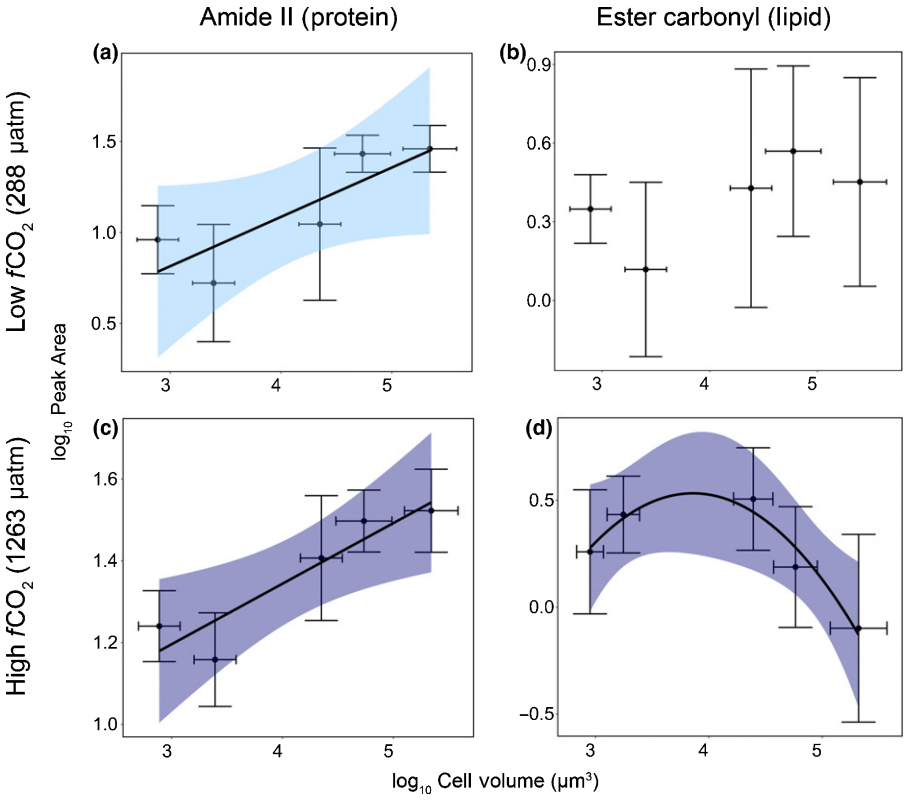

Fig. 7 Cell volume (µm³) and protein (amide II) or lipid (ester carbonyl) content; (a, b) for diatoms in the low fCO_2 treatment (288 µatm) and (c, d) high fCO_2 treatment (1263 µatm). Data have been $\log_{10}$ transformed and fitted with linear or a second order polynomial regression with 95% confidence intervals (shading). The data represent mean ± SD ($n > 19$), with all regressions applied to the mean.

between the lowest and highest fCO_2 concentrations measured, suggests protein availability for secondary production may increase under OA.

The measured changes in lipids and FA content in response to fCO_2 between taxa were more variable than those for protein. We found that increasing fCO_2 resulted in decreased relative lipid content for the larger diatoms compared with a bell-shaped increase in lipid content for the smaller diatoms *F. cylindrus* and *P. truncata*. Because the effect for *Chaetoceros* spp. closely followed growth rate, it is likely that the response was related to growth phase and/or nutrient limitation rather than fCO_2, limiting the interpretation of fCO_2 effects on macromolecular partitioning for *Chaetoceros* spp. particularly for M3 and M4 for which cells had reached stationary phase. These size-specific trends may be due to the larger diatoms in this study having a greater need to prioritise protein synthesis over lipid storage (although it is important to note that we did not differentiate between storage and structural lipid types in the analyses). In the two large discoid centric diatoms (*S. microtrias* and discoid centrics), the fCO_2-related decline in lipids was accompanied by an increase in relative protein content suggesting a shift in macromolecular energy partitioning with acidification. This loss in lipid content is congruent with a previous study that found that total FA content declined significantly in the discoid centric diatom *T. weissflogii* at high CO_2 (Rossoll *et al.*, 2012). An increase in protein content at the expense of ester carbonyl, could be explained by the fact that ester carbonyl acts as a fixed carbon reservoir for protein biosynthesis in cells (Terry *et al.*, 1985; Stehfest *et al.*, 2005). Therefore, its degradation and decline could be directly linked to increased protein production. Alternatively, changes to lipid content could be a strategy for regulating cell ballast. In a parallel study from the same mesocosm experiment, we measured significant declines in the silicification rates of these two taxa with acidification (Petrou *et al.*, 2019). We found that at the highest fCO_2 (M6) treatment, silicification declined 59% and 39% in *S. microtrias* and discoid centrics, respectively (Petrou *et al.*, 2019). Extent of silicification contributes to diatom sinking rate (Miklasz & Denny, 2010), and therefore any reduction in silicification may increase diatom buoyancy. By decreasing cellular lipid content, the diatoms may counteract this loss in ballast, increasing their density and, therefore, decreasing buoyancy (Smayda, 1970), enabling the diatoms to regulate their depth within the water column.

In both *P. truncata* and *F. cylindrus*, an fCO_2 threshold for increasing lipid content was observed, for which lipids increased until *c.* 950 µatm, after which they declined. This initial increase in lipid reserves at moderate fCO_2 enrichment, may reflect a boosted investment into energy stores, as the cells are relieved from potential carbon limitation (Halsey & Jones, 2015). However, as protein content continued to increase for both species beyond *c.* 950 µatm, the threshold response of lipid content probably indicates that, once the CCMs are saturated, lipids are preferentially catabolised for energy to synthesise proteins and support growth (Stehfest *et al.*, 2005; Halsey & Jones, 2015). Alternatively, the shift could be due to higher energy requirements to support increased proton pumping at high fCO_2 (Deppeler *et al.*, 2018). This shift towards higher energy consumption indicates that CO_2 concentrations > 1000 µatm, which are

predicted by 2100 (IPCC, 2014), could be a critical point of change for these species, a finding supported by our parallel mesocosm study (Deppeler *et al.*, 2018), which reported significant declines in carbon production by these taxa at fCO_2 concentrations > 1140 µatm.

Our inability to detect any NO_x by day 18 alerted us to the possibility of nitrogen limitation in our mesocosms, which has the potential to confound any fCO_2-induced macromolecular responses. Indeed, in three of the mesocosms, the NO_x concentrations were strongly diminished by day 16; M1, M3 (1.5 µM) and M4 (0.2 µM) (Deppeler *et al.*, 2018), yet while these concentrations are low for SO waters, they are within the normal range of most oceanic waters and not generally considered limiting for microalgae (Voss *et al.*, 2013). Notwithstanding these low NO_x values, our data did not exhibit signs of limitation. Instead, the diatoms studied were still actively growing on day 18 (except *Chaetoceros* spp. from M3 and M4) and therefore unlikely have been nutrient limited, possibly supported by luxury uptake of nitrate at an earlier stage (Behrenfeld *et al.*, 2021). Furthermore, support for the unlikelihood that our data were affected by nutrient limitation is provided by the fact that removal of the data points for the mesocosms in which nitrate concentrations were low on day 16 (M1, M3 and M4) had little or no effect on the observed trends.

If our snapshot of macromolecular profiles in response to fCO_2 enrichment is representative of the broader effect on phytoplankton nutritional quality in nature, selection for smaller diatoms (as was the case in our mesocosm community study, see Hancock *et al.*, 2018), with increased lipid and protein content per cell could translate to increased energy available for secondary production. Availability and transfer of lipids through the trophic web are particularly important, as lipids are the most energy-rich macromolecules, with an energy storage capacity of 39.4 J mg^{-1}, compared with 23.6 J mg^{-1} for proteins (Hagen & Auel, 2001). High lipid content in primary producers is essential to sustain growth, reproduction and ensure the survival of the aphotic Antarctic winter of higher trophic levels, from zooplankton to marine mammals and birds (Jones & Flynn, 2005; Klein Breteler *et al.*, 2005; Kattner *et al.*, 2007). Therefore, OA may result in higher secondary production. However, an increase in available lipid in small cells does not directly imply an increase in the calories transferred to higher trophic levels. Antarctic krill exhibit only 50% grazing efficiency for phytoplankton < 20 µm (Boyd & Heyraud, 1984; Quentin & Ross, 1985; Moline *et al.*, 2001), meaning a shift to a community dominated by small diatoms may have significant impacts on krill populations and the organisms that depend on them. Furthermore, krill and other large zooplankton have been demonstrated to have a grazing preference for larger cells (Meyer & El-Sayed, 1983; Quentin & Ross, 1985; Meyer *et al.*, 2003), which means that the decline in lipid measured in the larger diatoms in this study could directly affect large zooplankton populations. Indeed, copepod diets low in lipid content have been shown to cause significant declines in growth and fecundity (Shin *et al.*, 2003; Rossoll *et al.*, 2012). Considering the multiplicity of responses, the opposing effects of increased available lipid content have to be weighed up with overall changes to trophic efficiency, which will probably be influenced by a shift in community composition, a decrease or change in average cell size (Hancock *et al.*, 2018) and reduced silicification (Petrou *et al.*, 2019), all of which affect grazing preference and efficiency. As such, an increase in energy available to secondary production under OA will not necessarily translate to increased energy transferred to higher trophic levels.

Taking a single-cell approach, we were able to differentiate diatom species responses to OA with increasing fCO_2. We saw clear species-specific trends in macromolecular stores despite high within-treatment variability. The variability observed between diatom populations may be attributed to differences in cell size and, therefore, differences in cellular nutrient requirement (Sarthou *et al.*, 2005), cell shape, which can also affect diffusion rates (Pahlow *et al.*, 1997; Mitchell *et al.*, 2013) or some other underlying physiological variant, such as photosynthesis and carbon acquisition strategies (Hennon *et al.*, 2017), however, none of these parameters were tested here. Instead, this species-specific variability reveals the adaptive potential of each taxon and, therefore, the potential resilience of that taxon to environmental change. Similarly, the broad within-species spread in macromolecular responses suggests large phenotypic plasticity in the taxa studied. Interestingly, we saw a general decrease in within-treatment variability with increasing fCO_2, suggesting a possible convergence of cell responses and, therefore, potential for reduced within-species plasticity. Ecologically, this could have implications for resilience to environmental change in future populations. Contrary to the commonly observed shift towards larger cells, the highest fCO_2 levels of our community study selected for smaller diatoms (Hancock *et al.*, 2018). This loss of larger diatoms from the community could reduce the efficiency of energy transfer, as smaller cell sizes may be more difficult to graze on for some larger zooplankton. From a trophic energy perspective, reduced grazing efficiency or smaller krill populations due to a community dominated by smaller diatoms, despite a per cell increase in protein and lipid content, may in fact reduce the transfer efficiency of nutrients to higher predators (Fig. 8). This may be enhanced by concurrent sea surface temperature increases, which have been shown to contribute to polar phytoplankton communities being dominated by smaller cells (Mendes *et al.*, 2013, 2018; Coello-Camba *et al.*, 2014). Alternatively, when viewed in combination with reduced silicification in the taxonomic groups studied here, not only diatom sinking rates would be reduced, but also protection against grazing (Liu *et al.*, 2016), potentially increasing diatom predation in surface waters. Such a shift could counter some of the energy loss that might ensue with a trend towards a community dominated by smaller cells, while increasing recycling of carbon and silica via increased microbial loop activity. Deriving precise trophic projections based on the taxonomic variability in macromolecular responses described here is challenging due to the uncertainty around OA-driven changes to community composition and size structure. However, if our results hold true, they indicate that as the community becomes dominated by smaller, less silicified

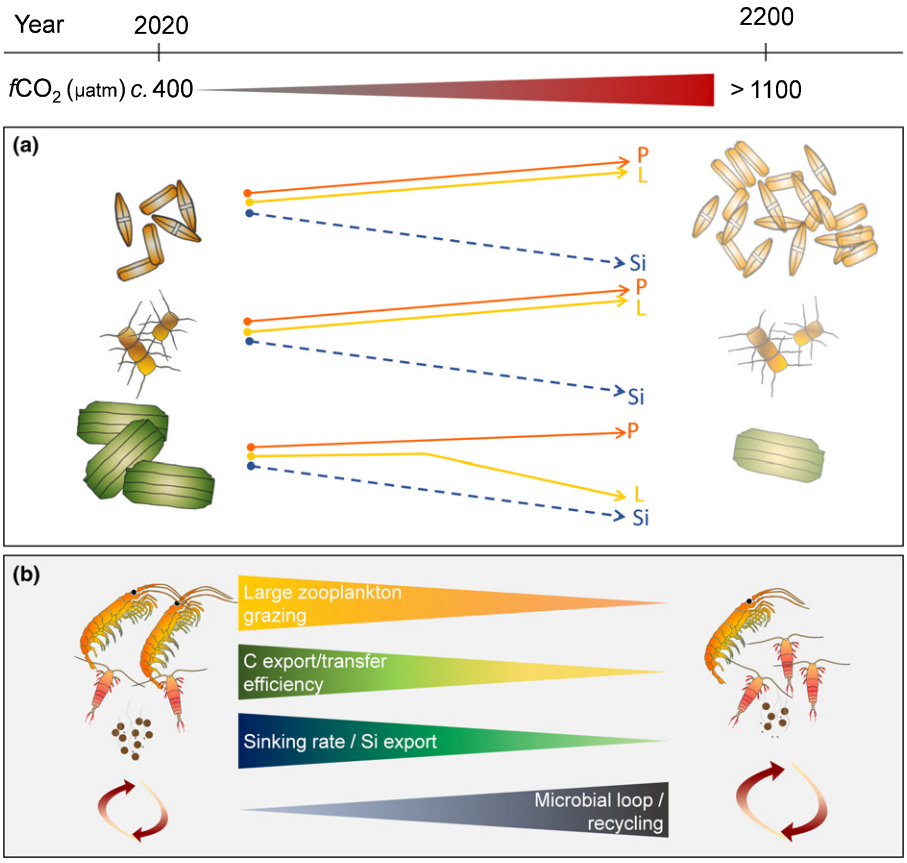

Fig. 8 Summary of measured changes to diatoms under high fCO_2 and expected ecological implications. (a) Projected increase in CO_2 by the end of next century (2200) results in a shift in dominance towards smaller diatom species with increased lipid and protein content, but reduced silicification, while larger diatoms become scarce with lower lipid content and reduced silica content. (b) These changes alter food quality and availability for large zooplankton species such as krill and large copepods, affecting zooplankton growth and fecundity. A reduction in large diatoms and large zooplankton grazing would be likely to reduce carbon and silica export efficiency and alter energy transfer through to higher trophic organisms. Lowered silica production may alleviate some of this loss by increasing grazing on the abundant lipid and protein rich small diatoms by smaller zooplankton. Smaller cells and high grazing rates by smaller zooplankton would probably increase microbial loop activity and nutrient recycling in surface waters. Solid lines represent measured changes to relative protein (P) and lipid (L) content, while dashed lines represent the measured decline in silicification (Si) in the same diatoms from a parallel study (Petrou *et al.*, 2019).

taxa under OA, the increased protein and lipid may benefit some grazers, but may not be as effectively conveyed to higher trophic levels due to overall less efficient large zooplankton grazing (Fig. 8). Concurrently, the remaining large taxa would have less lipid, resulting in less energy available to large zooplankton, with biogeochemical consequences of reduced carbon export and increased nutrient remineralisation (Fig. 8). Therefore, while determining that the net effects of OA on trophic energy transfer is inherently complex, it is clear that OA drives changes in diatom macromolecular partitioning with the potential for significant implications on nutrient and energy supply to the Antarctic pelagic food web.

Acknowledgements

We thank the Australian Synchrotron Principal Beamline Scientists Drs. Mark Tobin and Jitra-porn Vongsvivut for technical support in synchrotron IR microspectroscopy data acquisition. Part of this work was funded by the Australian Synchrotron through merit-based beamtime awarded on the Infrared Microscopy (IRM) beamline (AS153/IRM/10005) awarded to KP. Field support and sample collection was conducted as part of Australian Antarctic Science Project 4026 awarded to ATD. Samples were imported under permit no. IP13019928. RJD is supported by an Australian Government Research Training Program Scholarship and an AINSE Ltd. Postgraduate Research Award (PGRA), and research funding was provided by the School of Life Sciences, University of Technology Sydney. The authors declare that they have no conflict of interest.

Author contributions

RJD: formal analysis, data visualisation, writing original draft; DAN: data curation, formal analysis, writing review and editing; CES: investigation; SD: investigation, writing review and editing; AMH: investigation, writing review and editing; KGS: investigation, writing review and editing; ATD: conceptualisation, funding acquisition, investigation, writing review and editing; and KP: conceptualisation, methodology, investigation, data visualisation, supervision, funding acquisition, writing review and editing.

ORCID

Stacy Deppeler https://orcid.org/0000-0003-2213-2656
Rebecca J. Duncan https://orcid.org/0000-0003-2686-5654
Alyce M. Hancock https://orcid.org/0000-0001-6049-5592
Daniel A. Nielsen https://orcid.org/0000-0001-6678-5937
Katherina Petrou https://orcid.org/0000-0002-2703-0694
Kai G. Schulz https://orcid.org/0000-0002-8481-4639

Data availability

Data are available in Supporting Information and via the Australian Antarctic Division Data Centre (doi: 10.26179/ej5x-2h37).

References

Admiraal W, Peletier H, Laane RWPM. 1986. Nitrogen metabolism of marine planktonic diatoms; excretion, assimilation and cellular pools of free amino acids in seven species with different cell size. *Journal of Experimental Marine Biology and Ecology* **98**: 241–263.

Arrigo KR. 2005. Marine microorganisms and global nutrient cycles. *Nature* **437**: 349–355.

Bach TL, Taucher J. 2019. CO_2 effects on diatoms: a synthesis of more than a decade of ocean acidification experiments with natural communities. *Ocean Science* **15**: 1159–1175.

Bambery KR, Wood BR, McNaughton D. 2012. Resonant Mie scattering (RMieS) correction applied to FTIR images of biological tissue samples. *Analyst* **137**: 126–132.

Baragi LV, Khandeparker L, Anil AC. 2015. Influence of elevated temperature and pCO_2 on the marine periphytic diatom *Navicula distans* and its associated organisms in culture. *Hydrobiologia* **762**: 127–142.

Beardall J, Raven JA. 2004. The potential effects of global climate change on microalgal photosynthesis, growth and ecology. *Phycologia* **43**: 26–40.

Behrenfeld MJ, Halsey KH, Boss E, Karp-Boss L, Milligan AJ, Peers G. 2021. Thoughts on the evolution and ecological niche of diatoms. *Ecological Monographs* **91**: e01457.

Bellerby RGJ, Schulz KG, Riebesell U, Neill C, Nondal G, Heegaard E, Johannessen T, Brown KR. 2008. Marine ecosystem community carbon and nutrient uptake stoichiometry under varying ocean acidification during the PeECE III experiment. *Biogeosciences* **5**: 1517–1527.

Berge T, Daugbjerg N, Andersen BB, Hansen PJ. 2010. Effect of lowered pH on marine phytoplankton growth rates. *Marine Ecology Progress Series* **416**: 79–91.

Bhavya PS, Kim BK, Jo N, Kim K, Kang JJ, Lee JH, Lee D, Lee JH, Joo HT, Ahn SH *et al.* 2018. A review on the macromolecular compositions of phytoplankton and the implications for aquatic biogeochemistry. *Ocean Science Journal* **54**: 1–14.

Boyd CM, Heyraud M, Boyd CN. 1984. Feeding of the Antarctic Krill *Euphausia Superba*. *Journal of Crustacean Biology* **4**: 123–141.

Bromke MA. 2013. Amino acid biosynthesis pathways in diatoms. *Metabolites* **3**: 294–311.

Brussaard CPD, Noordeloos AAM, Witte H, Collenteur MCJ, Schulz K, Ludwig A, Riebesell U. 2013. Arctic microbial community dynamics influenced by elevated CO_2 levels. *Biogeosciences* **10**: 719–731.

Chen CY, Durbin EG. 1994. Effects of pH on the growth and carbon uptake of marine phytoplankton. *Marine Ecology Progress Series* **109**: 83–94.

Chen G, Zhao L, Qi Y. 2015. Enhancing the productivity of microalgae cultivated in wastewater toward biofuel production: a critical review. *Applied Energy* **137**: 282–291.

Coello-Camba A, Agustí S, Holding J, Arrieta JM, Duarte CM. 2014. Interactive effect of temperature and CO_2 increase in Arctic phytoplankton. *Frontiers in Marine Science* **49**: 1–10.

Cottingham KL, Lennon JT, Brown BL. 2005. Knowing when to draw the line: designing more informative ecological experiments. *Frontiers in Ecology and the Environment* **3**: 145–152.

Cowles TJ, Olson RJ, Chisholm SW. 1988. Food selection by copepods: discrimination on the basis of food quality. *Marine Biology* **100**: 41–49.

Davidson AT, McKinlay J, Westwood K, Thomson PG, Van Den Enden R, De Salas M, Wright S, Johnson R, Berry K. 2016. Enhanced CO_2 concentrations change the structure of Antarctic marine microbial communities. *Marine Ecology Progress Series* **552**: 93–113.

Denman KL, Brasseur G, Chidthaisong A, Ciais P, Cox P, Dickinson R, Hauglustaine D, Heinze C, Holland E, Jacob D *et al.* 2007. Couplings between changes in the climate system and biogeochemistry. In: Solomon S *et al.*, eds. *Climate change 2007: the physical science basis. Contribution of Working Group I to the fourth assessment report of the Intergovernmental Panel on Climate Change*. Cambridge, UK and New York, NY, USA: Cambridge University Press, 499–563.

Deppeler S, Petrou K, Schulz KG, Westwood K, Pearce I, McKinlay J, Davidson A. 2018. Ocean acidification of a coastal Antarctic marine microbial community reveals a critical threshold for CO_2 tolerance in phytoplankton productivity. *Biogeosciences* **15**: 209–231.

Deppeler SL, Davidson AT. 2017. Southern Ocean phytoplankton in a changing climate. *Frontiers in Marine Science* **4**: 40.

Dickson AG. 2010. Standards for Ocean measurements. *Oceanography* **23**: 34–47.

Dickson AG, Sabine CL, Christian JR. 2007. Guide to best practices for ocean CO_2 measurements. In: *PICES special publication 3, IOCCP report no. 8*. Sidney, BC, Canada: North Pacific Marine Science Organisation.

Dortch Q. 1982. Effect of growth conditions on accumulation of internal nitrate, ammonium, amino acids, and protein in three marine diatoms. *Journal of Experimental Marine Biology and Ecology* **61**: 243–264.

Eggers SL, Lewandowska AM, Barcelos e Ramos J, Blanco-Ameijeiras S, Gallo F, Matthiessen B. 2014. Community composition has greater impact on the functioning of marine phytoplankton communities than ocean acidification. *Global Change Biology* **20**: 713–723.

Engel A, Schulz KG, Riebesell U, Bellerby R, Delille B, Schartau M. 2008. Effects of CO_2 on particle size distribution and phytoplankton abundance during a mesocosm bloom experiment (PeECE II). *Biogeosciences* **5**: 509–521.

Feng Y, Hare CE, Leblanc K, Rose JM, Zhang Y, DiTullio GR, Lee PA, Wilhelm SW, Rowe JM, Sun J *et al.* 2009. Effects of increased pCO_2 and temperature on the north atlantic spring bloom. I. The phytoplankton community and biogeochemical response. *Marine Ecology Progress Series* **388**: 13–25.

Feng Y, Hare CE, Rose JM, Handy SM, DiTullio GR, Lee PA, Smith WO, Peloquin J, Tozzi S, Sun J *et al.* 2010. Interactive effects of iron, irradiance and CO_2 on Ross Sea phytoplankton. *Deep-Sea Research Part I: Oceanographic Research Papers* **57**: 368–383.

Finkel ZV, Follows MJ, Liefer JD, Brown CM, Benner I, Irwin AJ. 2016. Phylogenetic diversity in the macromolecular composition of microalgae. *PLoS ONE* **11**: e0155977.

Frölicher TL, Sarmiento JL, Paynter DJ, Dunne JP, Krasting JP, Winton M. 2015. Dominance of the Southern Ocean in anthropogenic carbon and heat uptake in CMIP5 models. *Journal of Climate* **28**: 862–886.

Gille ST. 2002. Warming of the Southern Ocean since the 1950s. *Science* **295**: 1275–1277.

Giordano M, Kansiz M, Heraud P, Beardall J, Wood B, McNaughton D. 2001. Fourier transform infrared spectroscopy as a novel tool to investigate changes in intracellular macromolecular pools in the marine microalga *Chaetoceros muellerii* (Bacillariophyceae). *Journal of Phycology* **37**: 271–279.

Graeve M, Kattner G, Hagen W. 1994. Diet-induced changes in the fatty acid composition of Arctic herbivorous copepods: experimental evidence of trophic markers. *Journal of Experimental Marine Biology and Ecology* **182**: 97–110.

Haberman KL, Ross RM, Quetin LB. 2003. Diet of the Antarctic krill (*Euphausia superba Dana*): II. Selective grazing in mixed phytoplankton assemblages. *Journal of Experimental Marine Biology and Ecology* **283**: 97–113.

Hagen W, Auel H. 2001. Seasonal adaptations and the role of lipids in oceanic zooplankton. *Zoology* **104**: 313–326.

Halsey KH, Jones BM. 2015. Phytoplankton strategies for photosynthetic energy allocation. *Annual Review of Marine Science* **7**: 265–297.

Hamm CE, Merkel R, Springer O, Jurkojc P, Maiert C, Prechtelt K, Smetacek V. 2003. Architecture and material properties of diatom shells provide effective mechanical protection. *Nature* **421**: 841–843.

Hancock AM, Davidson AT, McKinlay J, McMinn A, Schulz KG, Van Den Enden RL. 2018. Ocean acidification changes the structure of an Antarctic coastal protistan community. *Biogeosciences* **51**: 2393–2401.

Hancock AM, King CK, Stark JS, McMinn A, Davidson AT. 2020. Effects of ocean acidification on Antarctic marine organisms: a meta-analysis. *Ecology and Evolution* **10**: 4495–4514.

Havenhand J, Dupont S, Quinn GP. 2010. Designing ocean acidification experiments to maximise inference. In: Riebesell U *et al.*, eds. *Guide to best practices for ocean acidification research and data reporting*. Luxembourg City, Luxembourg: Publications Office of the European Union, 67–79.

Head EJH, Harris LR. 1994. Feeding selectivity by copepods grazing on natural mixtures of phytoplankton determined by HPLC analysis of pigments. *Marine Ecology Progress Series* **110**: 75–83.

Hennon GM, Ashworth J, Groussman RD, Berthiaume C, Morales RL, Baliga NS, Orellana MV, Armbrust EV. 2015. Diatom acclimation to elevated CO_2 via cAMP signalling and coordinated gene expression. *Nature Climate Change* **5**: 761–765.

Hennon GM, Limón MDH, Haley ST, Juhl AR, Dyhrman ST. 2017. Diverse CO_2-induced responses in physiology and gene expression among eukaryotic phytoplankton. *Frontiers in Microbiology* **8**: 2547.

Heraud P, Wood BR, Tobin MJ, Beardall J, McNaughton D. 2005. Mapping of nutrient-induced biochemical changes in living algal cells using synchrotron infrared microspectroscopy. *FEMS Microbiology Letters* **249**: 219–225.

Hillebrand H, Dürselen CD, Kirschtel D, Pollingher U, Zohary T. 1999. Biovolume calculation for pelagic and benthic microalgae. *Journal of Phycology* **35**: 403–424.

Hoppe CJM, Hassler CS, Payne CD, Tortell PD, Rost BR, Trimborn S. 2013. Iron limitation modulates ocean acidification effects on Southern Ocean phytoplankton communities. *PLoS ONE* **8**: e79890.

Hoppe CJM, Holtz LM, Trimborn S, Rost B. 2015. Ocean acidification decreases the light-use efficiency in an Antarctic diatom under dynamic but not constant light. *New Phytologist* **207**: 159–171.

Hoppe CJM, Schuback N, Semeniuk DM, Maldonado MT, Rost B. 2017. Functional redundancy facilitates resilience of subarctic phytoplankton assemblages toward ocean acidification and high irradiance. *Frontiers in Marine Science* **4**: 229.

Hussherr R, Levasseur M, Lizotte M, Tremblay JÉ, Mol J, Thomas H, Gosselin M, Starr M, Miller LA, Jarniková T *et al.* 2017. Impact of ocean acidification on Arctic phytoplankton blooms and dimethyl sulfide concentration under simulated ice-free and under-ice conditions. *Biogeosciences* **14**: 2407–2427.

Intergovernmental Panel on Climate Change (IPCC). 2014. *Climate change 2014: impacts, adaptation and vulnerability: Part B: Regional aspects: Working Group II contribution to the fifth assessment report of the Intergovernmental Panel on Climate*. Cambridge, UK: Cambridge University Press.

Jin P, Hutchins DA, Gao K. 2020. The impacts of ocean acidification on marine food quality and its potential food chain consequences. *Frontiers in Marine Science* **7**: 543979.

Jones RH, Flynn KJ. 2005. Nutritional status and diet composition affect the value of diatoms as copepod prey. *Science* **307**: 1457–1459.

Kang SH, Fryxell GA. 1993. Phytoplankton in the Weddell Sea, Antarctica: composition, abundance and distribution in water-column assemblages of the marginal ice-edge zone during austral autumn. *Marine Biology: International Journal on Life in Oceans and Coastal Waters* **116**: 335–348.

Kattner G, Hagen W, Lee RF, Campbell R, Deibel D, Falk-Petersen S, Graeve M, Hansen BW, Hirche HJ, Jónasdóttir SH *et al.* 2007. Perspectives on marine zooplankton lipids. *Canadian Journal of Fisheries and Aquatic Sciences* **64**: 1628–1639.

Khatiwala S, Primeau F, Hall T. 2009. Reconstruction of the history of anthropogenic CO_2 concentrations in the ocean. *Nature* **462**: 346–349.

Klein Breteler WCM, Schogt N, Rampen S. 2005. Effect of diatom nutrient limitation on copepod development: role of essential lipids. *Marine Ecology Progress Series* **291**: 125–133.

Kreyling J, Schweiger AH, Bahn M, Ineson P, Migliavacca M, Morel-Journel T, Christiansen JR, Schtickzelle N, Larsen KS. 2018. To replicate, or not to replicate – that is the question: how to tackle nonlinear responses in ecological experiments. *Ecology Letters* **21**: 1629–1638.

Kroeker KJ, Kordas RL, Crim R, Hendriks IE, Ramajo L, Singh GS, Duarte CM, Gattuso JP. 2013. Impacts of ocean acidification on marine organisms: quantifying sensitivities and interaction with warming. *Global Change Biology* **19**: 1884–1896.

Larsen JN, Anisimov OA, Constable A, Hollowed AB, Maynard N, Prestrud P, Prowse TD, Stone JMR. 2014. Polar regions. In: Barros VR *et al.*, eds. *Climate change 2014: impacts, adaptation, and vulnerability. Part B: Regional aspects. Contribution of Working Group II to the fifth assessment report of the Intergovernmental Panel on Climate Change*. Cambridge, UK: Cambridge University Press, 1567–1612.

Le Quéré C, Andrew RM, Friedlingstein P, Sitch S, Pongratz J, Manning AC, Korsbakken JI, Peters GP, Canadell JG, Jackson RB *et al.* 2018. Global carbon budget 2017. *Earth System Science Data* **10**: 405–448.

Lee R, Hagen W, Kattner G. 2006. Lipid storage in marine zooplankton. *Marine Ecology Progress Series* **307**: 273–306.

Litchman E, Klausmeier CA, Schofield OM, Falkowski PG. 2007. The role of functional traits and trade-offs in structuring phytoplankton communities: scaling from cellular to ecosystem level. *Ecology Letters* **10**: 1170–1181.

Liu H, Chen M, Zhu F, Harrison PJ. 2016. Effect of diatom silica content on copepod grazing, growth and reproduction. *Frontiers in Marine Science* **3**: 89.

Marañón E, Cermeño P, López-Sandoval DC, Rodríguez-Ramos T, Sobrino C, Huete-Ortega M, Blanco JM, Rodríguez J. 2013. Unimodal size scaling of phytoplankton growth and the size dependence of nutrient uptake and use. *Ecology Letters* **16**: 371–379.

Martin-Jézéquel V, Hildebrand M, Brzezinski MA. 2000. Silicon metabolism in diatoms: implications for growth. *Journal of Phycology* **36**: 821–840.

McNeil BI, Matear RJ. 2008. Southern Ocean acidification: a tipping point at 450-ppm atmospheric CO_2. *Proceedings of the National Academy of Sciences, USA* **105**: 18860–18864.

Mendes CRB, Tavano VM, Dotto TS, Kerr R, de Souza MS, Garcia CAE, Secchi ER. 2018. New insights on the dominance of cryptophytes in Antarctic coastal waters: a case study in Gerlache Strait. *Deep-Sea Research Part II: Topical Studies in Oceanography* **149**: 161–170.

Mendes CRB, Tavano VM, Leal MC, de Souza MS, Brotas V, Garcia CAE. 2013. Shifts in the dominance between diatoms and cryptophytes during three late summers in the Bransfield Strait (Antarctic Peninsula). *Polar Biology* **36**: 537–547.

Meyer B, Atkinson A, Blume B, Bathmann UV. 2003. Feeding and energy budgets of larval Antarctic krill *Euphausia superba* in summer. *Marine Ecology Progress Series* **257**: 167–177.

Meyer MA, El-Sayed SZ. 1983. Grazing of *Euphausia superba* Dana on natural phytoplankton populations. *Polar Biology* **1**: 193–197.

Miklasz KA, Denny MW. 2010. Diatom sinking speeds: improved predictions and insight from a modified Stoke's law. *Limnology and Oceanography* **55**: 2513–2525.

Mitchell JG, Seuront L, Doubell MJ, Losic D, Voelcker NH, Seymour J, Lal R. 2013. The role of diatom nanostructures in biasing diffusion to improve uptake in a patchy nutrient environment. *PLoS ONE* **8**: e59548.

Moline MA, Claustre H, Frazerj TK, Grzymskj JOE, Schofielly O, Verner M. 2001. Changes in phytoplankton assemblages along the Antarctic Peninsula and potential implications for the Antarctic food web. In: Davidson W *et al.*, eds. *Antarctic ecosystems: models for wider ecological understanding*. Christchurch, New Zealand: New Zealand Natural Sciences, 263–271.

Murdock JN, Wetzel DL. 2009. FT-IR microspectroscopy enhances biological and ecological analysis of algae. *Applied Spectroscopy Reviews* **44**: 335–361.

Nagelkerken I, Goldenberg SU, Ferreira CM, Ullah H, Connell SD. 2020. Trophic pyramids reorganize when food web architecture fails to adjust to ocean change. *Science* **369**: 829–832.

Nielsen LT, Jakobsen HH, Hansen PJ. 2010. High resilience of two coastal plankton communities to twenty-first century seawater acidification: evidence from microcosm studies. *Marine Biology Research* **6**: 542–555.

Pahlow M, Riebesell U, Wolf-Gladrow A. 1997. Impact of cell shape and chain formation on nutrient acquisition by marine diatoms. *Limnology and Oceanography* **42**: 1660–1672.

Paul AJ, Bach LT. 2020. Universal response pattern of phytoplankton growth rates to increasing CO_2. *New Phytologist* **228**: 1710–1716.

Petrou K, Baker KG, Nielsen DA, Hancock AM, Schulz KG, Davidson AT. 2019. Acidification diminishes diatom silica production in the Southern Ocean. *Nature Climate Change* **9**: 781–786.

Petrou K, Nielsen DA, Heraud P. 2018. Single-cell biomolecular analysis of coral algal symbionts reveals opposing metabolic responses to heat stress and expulsion. *Frontiers in Marine Science* **5**: doi: 10.3389/fmars.2018.00110.

Quentin LB, Ross RM. 1985. Feeding by Antarctic krill, *Euphausia superba*: does size matter? In: Siegfried WR, Condy PR, Laws RM, eds. *Antarctic nutrient cycles and food webs*. Berlin/Heidelberg, Germany: Springer, 372–377.

R Core Team. 2021. *R: a language and environment for statistical computing*. Vienna, Austria: R Foundation for Statistical Computing.

Riebesell U, Gattuso JP. 2015. Lessons learned from ocean acidification research. *Nature Climate Change* **5**: 12–14.

Ross PM, Parker L, O'Connor WA, Bailey EA. 2011. The impact of ocean acidification on reproduction, early development and settlement of marine organisms. *Water* **3**: 1005–1030.

Rossoll D, Bermúdez R, Hauss H, Schulz KG, Riebesell U, Sommer U, Winder M. 2012. Ocean acidification-induced food quality deterioration constrains trophic transfer. *PLoS ONE* **7**: e34737.

Ruess L, Müller-Navarra DC. 2019. Essential biomolecules in food webs. *Frontiers in Ecology and Evolution* **7**: 269.

Sabine CL, Feely RA, Gruber N, Key RM, Lee K, Bullister JL, Wanninkhof R, Wong CS, Wallace DWR, Tilbrook B *et al.* 2004. The oceanic sink for anthropogenic CO_2. *Science* **305**: 367–371.

Sackett O, Armand L, Beardall J, Hill R, Doblin M, Connelly C, Howes J, Stuart B, Ralph P, Heraud P. 2014. Taxon-specific responses of Southern Ocean diatoms to Fe enrichment revealed by synchrotron radiation FTIR microspectroscopy. *Biogeosciences* **11**: 5795–5808.

Sackett O, Petrou K, Reedy B, De Grazia A, Hill R, Doblin M, Beardall J, Ralph P, Heraud P. 2013. Phenotypic plasticity of Southern Ocean diatoms: key to success in a sea ice habitat? *PLoS ONE* **8**: e81185.

Sackett O, Petrou K, Reedy B, Hill R, Doblin M, Beardall J, Ralph P, Heraud P. 2016. Snapshot prediction of carbon productivity, carbon and protein content in a Southern Ocean diatom using FTIR spectroscopy. *ISME Journal* **10**: 416–426.

Sarthou G, Timmermans KR, Blain S, Tréguer P. 2005. Growth physiology and fate of diatoms in the ocean: a review. *Journal of Sea Research* **53**: 25–42.

Schneider CA, Raspnad WS, Eliceiri KW. 2012. NIH image to ImageJ: 25 years of image analysis. *Nature Methods* **9**: 671–679.

Shapiro SS, Wilk MB. 1965. An analysis of variance test for normality (complete samples). *Biometrika* **52**: 591–611.

Sheehan C, Nielsen D, Petrou K. 2020. Macromolecular composition, productivity and dimethylsulfoniopropionate in Antarctic pelagic and sympagic microalgal communities. *Marine Ecology Progress Series* **640**: 45–61.

Shi Q, Xiahou W, Wu H. 2017. Photosynthetic responses of the marine diatom *Thalassiosira pseudonana* to CO_2-induced seawater acidification. *Hydrobiologia* **788**: 361–369.

Shin K, Jang M-C, Jang P-K, Ju S-J, Lee T-K, Chang M. 2003. Influence of food quality on egg production and viability of the marine planktonic copepod *Acartia omorii*. *Progress in Oceanography* **57**: 265–277.

Smayda T. 1970. The suspension and sinking of phytoplankton in the sea. *Oceanography and Marine Biology: An Annual Review* **8**: 353–414.

Stehfest K, Toepel J, Wilhelm C. 2005. The application of micro-FTIR spectroscopy to analyze nutrient stress-related changes in biomass composition of phytoplankton algae. *Plant Physiology and Biochemistry* **43**: 717–726.

Stevens A, Ramirez-Lopez L. 2013. An introduction to the prospectr package. R package v.013. [WWW document] URL https://CRAN.R-project.org/package=prospectr [accessed 10 April 2020].

Sugie K, Fujiwara A, Nishino S, Kameyama S, Harada N. 2020. Impacts of temperature, CO_2, and salinity on phytoplankton community composition in the Western Arctic Ocean. *Frontiers in Marine Science* **6**: 821.

Terry KL, Hirata J, Laws EA. 1985. Light-, nitrogen-, and phosphorus-limited growth of *Phaeodactylum tricornutum* Bohlin strain TFX-1: chemical composition, carbon partitioning, and the diel periodicity of physiological processes. *Journal of Experimental Marine Biology and Ecology* **86**: 85–100.

Tew KS, Kao YC, Ko FC, Kuo J, Meng PJ, Liu PJ, Glover DC. 2014. Effects of elevated CO_2 and temperature on the growth, elemental composition, and cell size of two marine diatoms: potential implications of global climate change. *Hydrobiologia* **741**: 79–87.

Tobin MJ, Puskar L, Barber RL, Harvey EC, Heraud P, Wood BR, Bambery KR, Dillon CT, Munro KL. 2010. FTIR spectroscopy of single live cells in aqueous media by synchrotron IR microscopy using microfabricated sample holders. *Vibrational Spectroscopy* **53**: 34–38.

Tortell PD, Payne CD, Li Y, Trimborn S, Rost B, Smith WO, Riesselman C, Dunbar RB, Sedwick P, DiTullio GR. 2008. CO_2 sensitivity of Southern Ocean phytoplankton. *Geophysical Research Letters* **35**: L04605.

Tréguer P, Bowler C, Moriceau B, Dutkiewicz S, Gehlen M, Aumont O, Bittner L, Dugdale R, Finkel Z, Iudicone D *et al.* 2018. Influence of diatom diversity on the ocean biological carbon pump. *Nature Geoscience* **11**: 27–37.

Turner JT, Ianora A, Miralto A, Laabir M, Esposito F. 2001. Decoupling of copepod grazing rates, fecundity and egg-hatching success on mixed and alternating diatom and dinoflagellate diets. *Marine Ecology Progress Series* **220**: 187–199.

Urabe J, Togari J, Elser JJ. 2003. Stoichiometric impacts of increased carbon dioxide on a planktonic herbivore. *Global Change Biology* **9**: 818–825.

Vongsvivut J, Heraud P, Zhang W, Kralovec JA, McNaughton D, Barrow CJ. 2012. Quantitative determination of fatty acid compositions in micro-encapsulated fish-oil supplements using Fourier transform infrared (FTIR) spectroscopy. *Food Chemistry* **135**: 603–609.

Voss M, Bange HW, Dippner JW, Middelburg JJ, Montoya JP, Ward B. 2013. The marine nitrogen cycle: recent discoveries, uncertainties and potential relevance of climate change. *Philosophical Transactions of the Royal Society of London. Series B: Biological Sciences* **368**: 20130121.

Wagner H, Liu Z, Langner U, Stehfest K, Wilhelm C. 2010. The use of FTIR spectroscopy to assess quantitative changes in the biochemical composition of microalgae. *Journal of Biophotonics* **3**: 557–566.

Wickham H. 2009. *ggplot2: elegant graphics for data analysis*. R package v.2.2.1. [WWW document] URL https://ggplot2.tidyverse.org [accessed 10 April 2020].

Wickham H, François R, Henry L, Müller K. 2020. *dplyr: a grammar of data manipulation*. R package v.1.0.0. https://cran-r-project.org/package=dplyr [accessed 10 April 2020].

Wolf C, Frickenhaus S, Kilias ES, Peeken I, Metfies K. 2013. Regional variability in eukaryotic protist communities in the Amundsen Sea. *Antarctic Science* **25**: 741–751.

Wright SW, van den Enden RL, Pearce I, Davidson AT, Scott FJ, Westwood KJ. 2010. Phytoplankton community structure and stocks in the Southern Ocean (30–80°E) determined by CHEMTAX analysis of HPLC pigment signatures. *Deep-Sea Research Part II: Topical Studies in Oceanography* **57**: 758–778.

Wu Y, Gao K, Riebesell U. 2010. CO_2-induced **seawater acidification affects physiological performance of the marine diatom *Phaeodactylum tricornutum*.** *Biogeosciences* **7**: 2915–2923.

Supporting Information

Additional Supporting Information may be found online in the Supporting Information section at the end of the article.

Table S1 Summary of initial seawater (T0) conditions and mesocosm conditions on day 18.

Table S2 Summary of number of cells, per taxa, per mesocosm, measured for species-specific macromolecular content using Fourier transform infrared microspectroscopy.

Table S3 Cell density and community photosynthetic efficiency on day 18.

Table S4 Mean cell volume (μm^3) on day 18 for taxa from mesocosm 1 (M1) and mesocosm 6 (M6).

Table S5 Statistical output of the species-specific regression models (Figs 1–5).

Table S6 Statistical output of the lipid (ester carbonyl) to protein (amide II) ratio models (Fig. 6).

Table S7 Data corresponding to cell volume (μm^3) and protein (amide II) or lipid (ester carbonyl) content.

Table S8 Statistical output of the cell volume (μm^3) and protein (amide II) or lipid (ester carbonyl) content models (Fig. 7).

Please note: Wiley Blackwell are not responsible for the content or functionality of any Supporting Information supplied by the authors. Any queries (other than missing material) should be directed to the *New Phytologist* Central Office.